
EXTREMELY LOW THERMAL RESISTANCE ARCHITECTURES FOR $\text{Al}_x\text{Ga}_{1-x}$ SEMICONDUCTOR DEVICES

Kidus Guye¹, Davide Orlandini², Seunghoon Shin², Andy Allerman³, Damena Agonafer¹, Siddharth Rajan²,

Samuel Graham^{*1}

¹Department of Mechanical Engineering, University of Maryland, College Park

²Department of Electrical and Computer Engineering, The Ohio State University, Columbus

³Sandia National Laboratories, Albuquerque

*samuelg@umd.edu

ABSTRACT

Next-generation high-power radio-frequency (RF) devices increasingly demand transistors that operate efficiently with high gain at high frequencies. High-aluminum-content ultra-wide-bandgap (UWBG) AlGa_N alloys have shown great potential for enabling such high-frequency RF technologies. However, the widespread adoption of AlGa_N-based RF devices is limited by thermal-management challenges arising from the intrinsically low thermal conductivity of AlGa_N, which leads to higher device thermal resistance for a given geometry compared to Ga_N RF devices. As a result, these next-generation devices are highly susceptible to self-heating. This study investigates the thermal behavior of UWBG AlGa_N devices, focusing on the effects of AlGa_N channel thickness, substrate technology, and high-k material integration on reducing device thermal resistance to enable high-power operation. Experimental results demonstrate a record-low thermal resistance of 3.96 mm·K/W when an AlN substrate is employed and the AlGa_N channel thickness is reduced to 5 nm. These findings provide valuable insights into mitigating thermal limitations in UWBG devices through device-level engineering and strategic integration of high-k materials.

Keywords AlGa_N devices · RF devices · Thermal management · UWBG · AlN.

1 Introduction

Ultra-wide-bandgap (UWBG) semiconductor devices have emerged as promising candidates to meet the escalating performance demands of next-generation high-power and high-frequency electronics [1]. Among emerging materials, aluminum-rich AlGa_N alloys have shown strong potential for next-generation radio-frequency (RF) transistors, offering superior high-frequency and high-voltage capabilities [2]. This performance advantage arises from their UWBG (>5 eV), which enables higher breakdown fields and sustained high electron saturation velocity, resulting in a Johnson figure of merit (JFOM) that surpasses that of Ga_N-based devices (for example, Al_{0.85}Ga_{0.15}N exhibits a silicon-normalized JFOM of 81 compared to 30 for Ga_N) [3, 4, 5, 6]. However, these electrical advantages are offset by poor thermal performance. The thermal conductivity of AlGa_N is up to 21 times lower than that of Ga_N ($k_{\text{Ga}_x\text{N}_{1-x}} = 180 \text{ W}/(\text{m}\cdot\text{K})$) for Al compositions between 0.2 and 0.8 [7], which limits heat dissipation and leads to severe self-heating, ultimately affecting device performance and reliability.

Thermal management remains a critical design challenge for high-power semiconductor devices. Prior studies have shown that device-level engineering can reduce thermal impedance through optimized layer architecture, substrate selection, and improved interface quality. For Ga_N-based wide-bandgap devices (WBG), significant progress has been achieved by reducing channel temperature through buffer-layer and substrate engineering [8, 9, 10, 11]. Aller *et al.* reported a record-low thermal boundary resistance (TBR) of 3.4 m²K/(GW) across nanocrystalline diamond/AlGa_N interfaces, demonstrating the effectiveness of diamond as a heat-spreading layer [12]. Tsurumi *et al.* found that replacing conventional Si_N passivation with AlN significantly enhanced lateral heat spreading in AlGa_N/Ga_N HFETs [13]. Hirama

et al. achieved a thermal resistance as low as 4.1 K-mm/W using single-crystal diamond substrates in AlGaIn/GaN High Electron Mobility Transistors (HEMTs), underscoring the benefits of high-thermal-conductivity substrates [14]. Alam *et al.* demonstrated that incorporating thick AlN heat-spreading layers into Al_{0.26}Ga_{0.74}N/GaN HEMTs reduced thermal resistance by more than a factor of 2 compared to devices without a heat spreader [15]. Likewise, additional numerical studies showed that double-sided diamond cooling can substantially lower channel temperature in β -Ga₂O₃ devices [16]. Similarly, a reduction in thermal resistance by a factor of 3 has been reported for AlGaIn channel devices using single-crystal AlN substrates compared to AlN/sapphire configurations [17]. Despite these advances, the thermal resistance of AlGaIn devices remains relatively high, and limited research has directly addressed the intrinsic thermal limitations of these low- k , high-power UWBG materials. To enable AlGaIn alloys for next-generation RF applications, effective thermal management strategies must be developed.

In this study, we demonstrate that channel and substrate engineering are important in providing a thermal solution to help mitigate the thermal challenges in AlGaIn UWBG devices. Device architectures with varying channel thicknesses are compared to evaluate the effect of channel scaling on thermal resistance and electrical behavior. To further assess the influence of substrate material, identical device architectures are fabricated on both sapphire and AlN substrates. Numerical simulations and experimental measurements are conducted to analyze the impact of channel and substrate design under steady-state and transient operating conditions. The device featuring a thin (5 nm) channel on an AlN substrate exhibited a record-low thermal resistance of 3.96 K-mm/W, representing a significant improvement in the heat dissipation capability.

2 Device Description

Four two-finger AlGaIn heterostructure field effect transistors (HFETs) were fabricated on both sapphire and AlN substrates, featuring AlGaIn channel thicknesses of 5 nm (AlGaIn-5-on-sapphire and AlGaIn-5-on-AlN) and 500 nm (AlGaIn-500-on-sapphire and AlGaIn-500-on-AlN). The schematic structures of the fabricated AlGaIn HFETs with 500 nm channel thickness and 5 nm channel thickness are illustrated, respectively, in Figure 1a and 1b, with a simplified thermal resistance network across the layers. Two epitaxial structures were grown on a TNSC-4000HT metal-organic chemical vapor deposition (MOCVD) reactor on both sapphire and AlN substrates. The first epitaxial structure consists, from bottom to top, of a thick AlN buffer layer; a 500 nm Al_{0.68}Ga_{0.32}N channel layer; a 43 nm Al_{0.82}Ga_{0.18}N split-doped barrier layer; and a 60 nm reverse-graded contact layer with the Al composition graded from Al_{0.83}Ga_{0.17}N to Al_{0.14}Ga_{0.86}N. The exact function and mechanism of the split-doped barrier layer are described in [18]. The second epitaxial structure includes the same epitaxial layers (reverse-graded contact layers, split-doped barrier layer, and buffer layer), but features a 5 nm ultra-thin unintentionally doped (UID) Al_{0.68}Ga_{0.32}N channel layer. Four main fabrication steps were performed on both epitaxial wafers to obtain the HFET devices shown in Figure 1a and 1b: (1) contact layer etching (targeted etching depth of 73 nm), (2) mesa isolation etching (targeted etching depth of 200 nm), (3) source/drain metal deposition (Ti/Al/Ni/Au = 20/120/30/100 nm), and (4) gate metal and gate-resistance thermometry (GRT) structure deposition (Ni/Au = 30/100 nm). **Figure 2a** and **2b** show the measured output characteristics for AlN-substrate devices.

The sheet resistance (R_{Sh}), the total sheet charge density (n_s), and the 2DEG electron mobility (μ_n) were estimated through Hall-effect measurements performed on Van der Pauw structures fabricated on each sample. The extracted values are summarized in Table 1. The mobility and charge in the thin AlGaIn-channel devices are lower, possibly due to interfacial impurities or uncompensated interface polarization charge. Recent work on thin-AlGaIn channel devices [19] suggests that, with appropriate growth conditions, thin buffer layers can still have high mobility (> 200 cm²/Vs).

Sample	R_{Sh} (k Ω / \square)	n_s (cm ⁻²)	μ_n (cm ² /Vs)
AlGaIn-500-on-sapphire	4.16	1.22×10^{13}	122
AlGaIn-5-on-sapphire	8.68	8.67×10^{12}	83
AlGaIn-500-on-AlN	6.19	8.75×10^{12}	116
AlGaIn-5-on-AlN	19.27	6.42×10^{12}	50

Table 1: Summary of sheet resistance (R_{Sh}), total sheet charge density (n_s), and 2DEG electron mobility (μ_n) extracted from Hall-effect measurements on the four samples.

2.1 Device Thermal Analysis

To characterize the thermal performance of each device, GRT, an electrical technique that measures temperature based on variations in gate metal resistance, is employed [20]. A four-terminal GRT structure is fabricated for each device, as

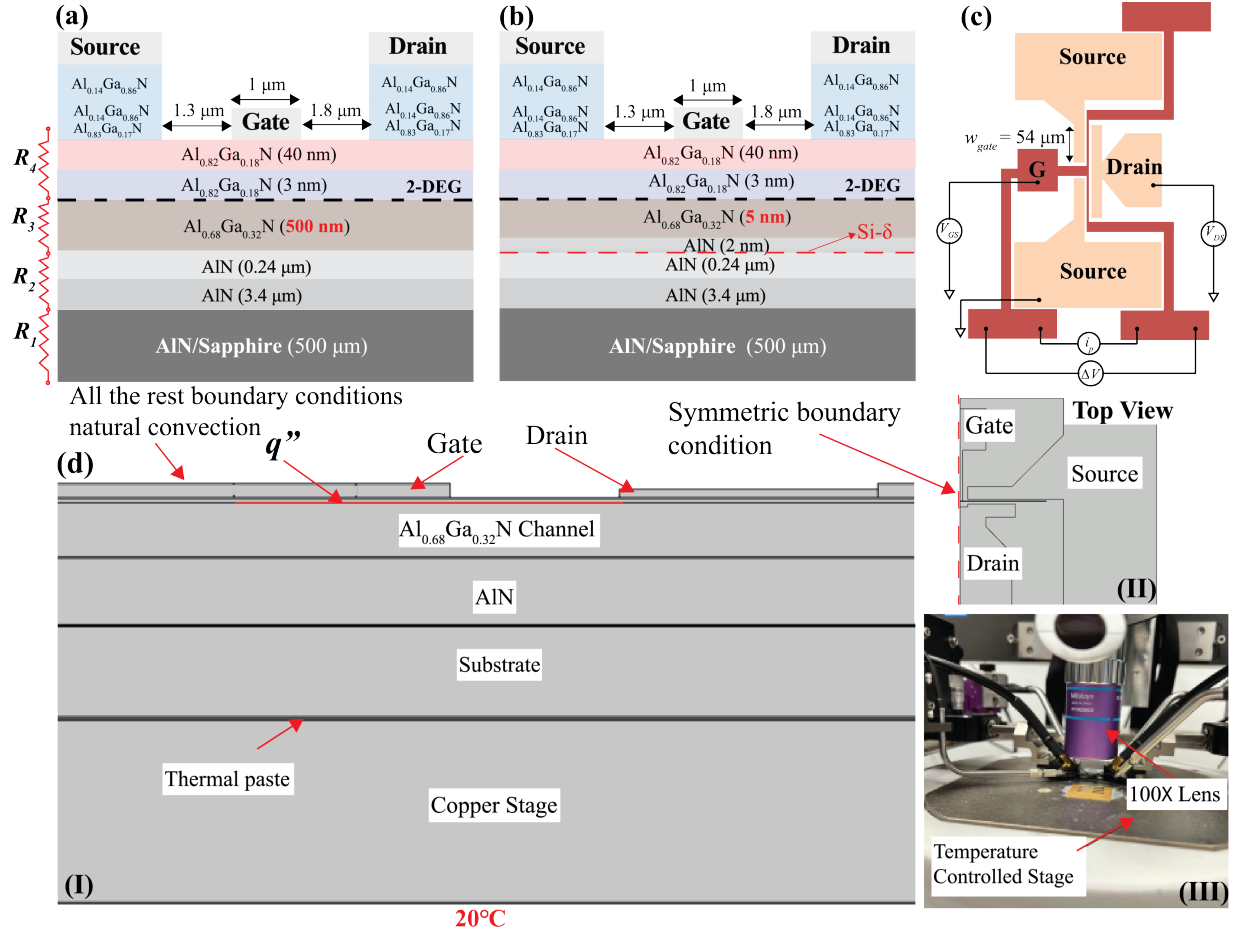


Figure 1: Cross-sectional schematic diagrams of the AlGaIn HEMT devices: (a) thick-channel device with a 500 nm channel fabricated on AlN (AlGaIn-500-on-AlN) and sapphire (AlGaIn-500-on-sapphire) substrates with a simplified thermal resistance networks across the layers where R_1 is the resistance across the substrate, R_2 is the combined resistance across the buffer layer, R_3 is the resistance across the channel, and R_4 is the resistance across the barrier layers, and (b) thin-channel device with a 5 nm channel fabricated on AlN (AlGaIn-5-on-AlN) and sapphire (AlGaIn-5-on-sapphire) substrates. (c) Schematic illustration of the gate resistance thermometry (GRT) design used for thermal characterization. (d) Numerical setup, (I) the schematics the numerical setup with all the boundary conditions, (II) top view of the source, drain and gate in the numerical setup, (III) image of the experimental setup on the SanjSCOPETMEZ500 with the 100X objective lens.

shown in Figure 1c. A probe current (i_p) is supplied through the GRT metal pads, and the voltage drop across (ΔV) the gate finger is measured using a separate set of probes. The GRT resistance is calibrated over a range of temperatures using a temperature-controlled stage to determine the temperature coefficient of resistance (TCR) [20]. A thermocouple was positioned on the die to improve the accuracy of the die temperature measurements during calibration. After calibration, the TCR was extracted from the resistance–temperature relationship and subsequently used to correlate the temperature rise in the gate metal with changes in its electrical resistance. The gate resistance was then measured at different operational power densities, and the corresponding temperature rise in each device was calculated using the extracted TCR. Each device was biased using ground–signal–ground (GSG) probes to apply the drain-to-source voltage (V_{DS}) and gate-to-source voltage (V_{GS}). A numerical thermal model for each device was developed using COMSOL Multiphysics to compare with the experimental results. A heat-flux boundary condition was applied at the 2-DEG region of the device channel, while a constant-temperature boundary condition of 20 °C was imposed at the bottom of the chuck to replicate the experimental stage conditions. All remaining surfaces were assigned natural convection boundary conditions with a heat transfer coefficient (h) of 10 W/(m²·K).

The GRT measurement results for the four devices are shown in Figure 3. The data present the average temperature rise across the gate region as a function of power density. To enable a clearer comparison among the different devices, the

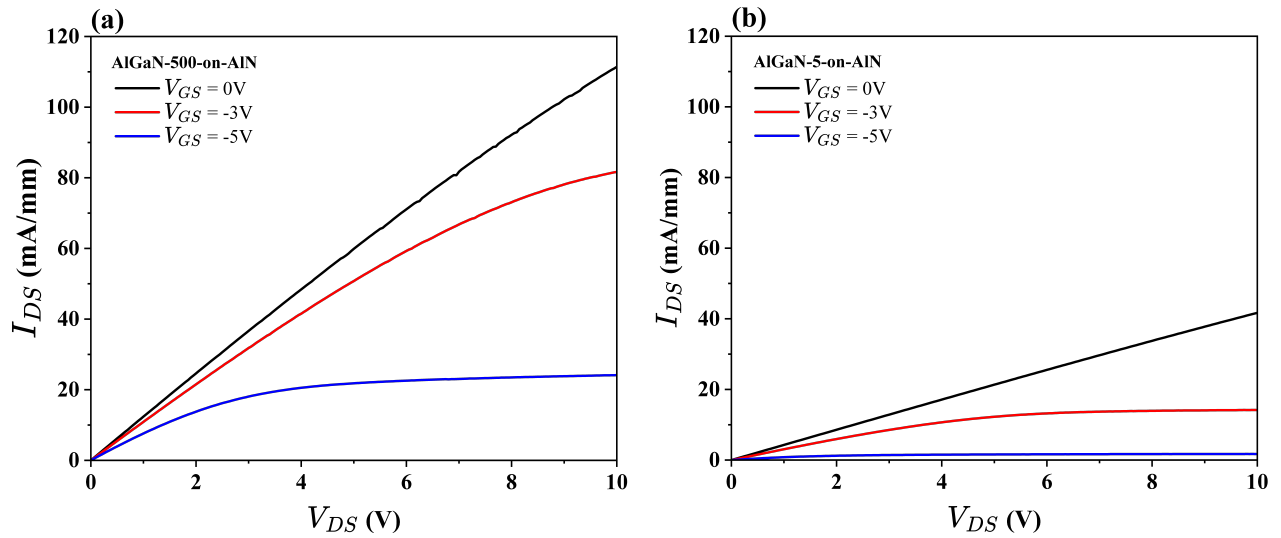


Figure 2: Output characteristics of the fabricated HFET devices: (a) a 500 nm AlGaIn channel on AlN (AlGaIn-500-on-AlN) and (b) a 5 nm AlGaIn channel on AlN (AlGaIn-5-on-AlN). For each device, the drain current I_D was measured by sweeping the drain-to-source voltage V_{DS} from 0 to 10 V under gate-to-source voltages V_{GS} of 0 V, -3 V and -5 V.

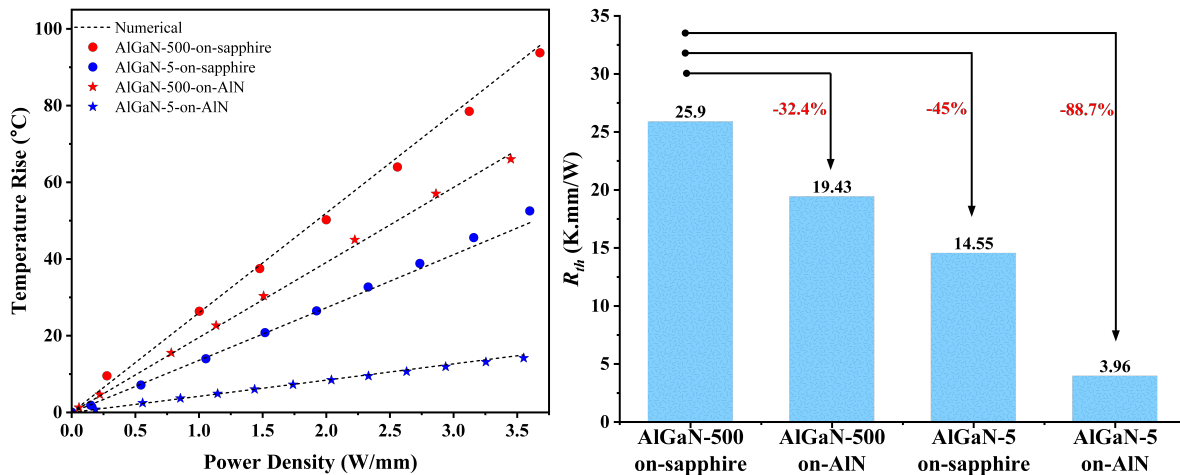


Figure 3: (a) Comparison of the average temperature rise across the gate metal for different power densities for the four different devices with their respective numerical model results. (b) The respective thermal resistance comparison between the four devices.

thermal resistance was calculated, as shown in Figure 3b. The 500 nm thick channel device on a sapphire substrate exhibits the poorest thermal performance, with a thermal resistance of 25.9 K·mm/W. This degradation is attributed to the low thermal conductivity of sapphire (increased in R_4), which limits heat conduction through the substrate to the heat sink, along with increased thermal resistance across the thick channel layer (R_3). For the same device architecture, replacing the sapphire substrate with AlN, a high- k material, significantly enhances heat dissipation, reducing the overall thermal resistance by more than 32%.

Another approach to enhance the thermal performance of AlGaIn-based devices is through channel engineering. Owing to the intrinsically low thermal conductivity of AlGaIn, reducing the channel thickness effectively decreases the thermal resistance contribution from this layer (R_3). As the channel corresponds to the primary heat-generation region, reducing its thermal resistance improves heat spreading and lowers the overall device thermal resistance. Accordingly, the channel thickness was reduced from 500 nm to 5 nm. The results indicate that, on a sapphire substrate, the total thermal resistance decreases by 45% to 14.55 K·mm/W compared to the thick-channel device. Furthermore, combining the thin

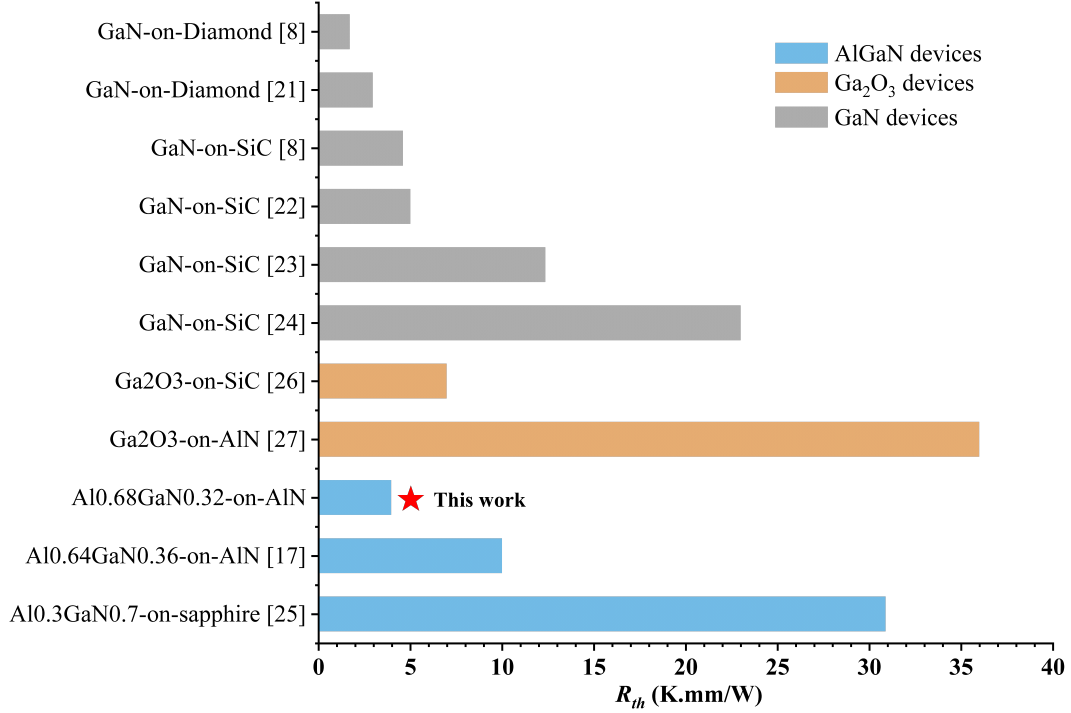


Figure 4: Comparison of thermal resistance value from this work and with reported work for GaN [21, 22, 8, 23, 24], AlGaN [17, 25] and Ga₂O₃ [26, 27] devices.

(5 nm) channel with an AlN substrate yielded a record-low thermal resistance of 3.96 K·mm/W, an 88.7% reduction, representing the lowest value reported for AlGaN devices to date, to the best of the authors' knowledge.

Figure 4 compares the thermal resistance values from this study with previously reported results for GaN and Ga₂O₃ devices using various thermal management strategies. The results indicate that the thermal resistance achieved in this work is comparable to that of GaN devices on SiC substrates. Furthermore, the recorded thermal resistance exhibits better thermal performance than similar UWBG devices, such as Ga₂O₃ transistors fabricated on SiC.

2.2 Transient Thermal Response

To further investigate the transient thermal behavior of the devices, surface temperature mapping is performed using transient thermoreflectance imaging (TTI). The TTI measurements were carried out with a SanjSCOPETMMEZ500 system using a 100X objective lens. This technique is based on the principle that the reflectivity (R) of a material changes for a given change in temperature (ΔT) given by 1. During calibration, a 530 nm pulsed LED excitation source was employed to record the variation in reflectance as a function of temperature [28]. From the calibration, the coefficient of thermoreflectance (C_{th}) was determined and subsequently used during measurements to generate spatially resolved temperature maps across the device surface.

$$C_{th} = \Delta T \times \left(\frac{\Delta R}{R} \right)^{-1}. \quad (1)$$

For the transient study, the devices were biased using an AMCAD pulsed I-V system with a square pulse resulting in a power density of 3.35 ± 0.15 W/mm, for a duty cycle of 25% and a total time period of 400 μ s. The results were averaged over 80 s, and the 95% confidence interval was calculated to estimate the uncertainty.

Figure 5 shows the experimental results, which are compared with numerical simulations performed under the same boundary conditions described earlier. The temperature was averaged across the gate surface near the center region (Figure 5a). The data show a clear reduction in temperature rise when transitioning to a thin channel, regardless of the substrate material. The AlGaIn-5-on-AlN device exhibits the lowest temperature among all HEMTs, consistent with the steady-state results (Figure 5a). This trend is also evident in the thermoreflectance image taken at 97.3 μ s,

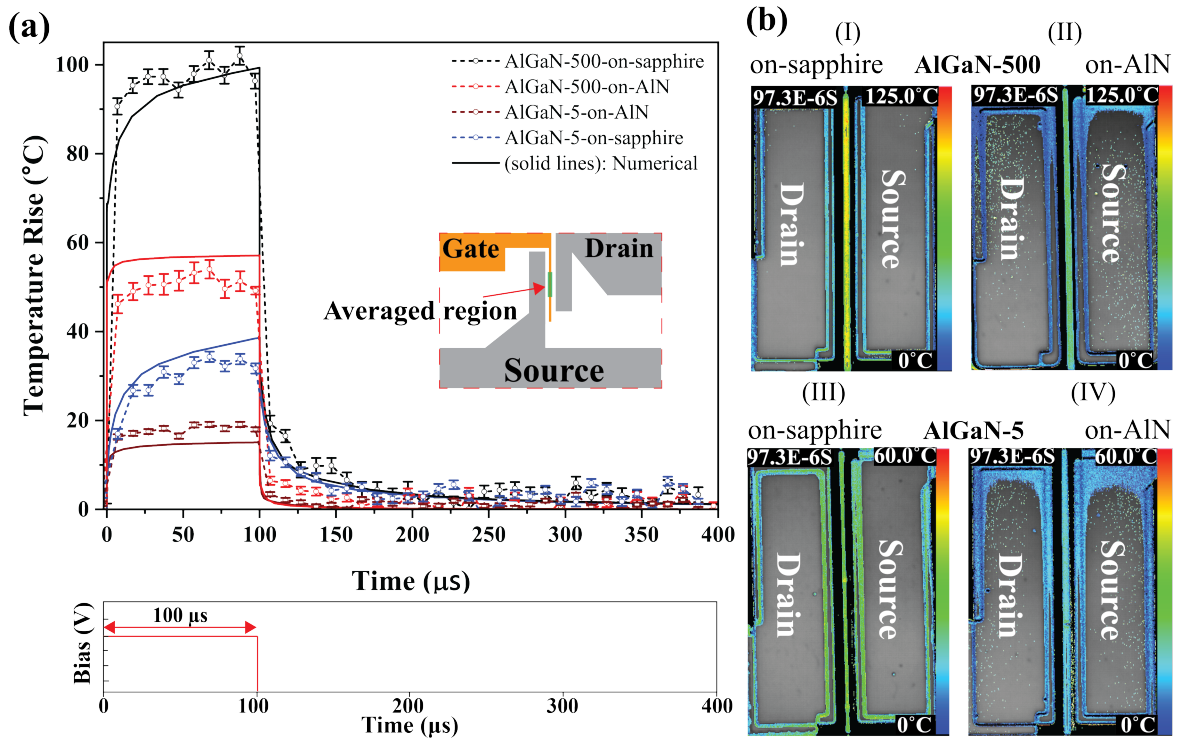


Figure 5: (a) Transient thermal response showing the temperature rise versus time for the four devices under a 25% duty cycle with a 400 μs period at a power density of 3.35 ± 0.15 W/mm. The solid lines represent the corresponding numerical simulation results for each device. (b) Thermoreflectance imaging illustrating the temperature rise at 97.3 μs for (I) AlGaIn-500-on-sapphire, (II) AlGaIn-500-on-AlN, (III) AlGaIn-5-on-sapphire, and (IV) AlGaIn-5-on-AlN. Note: The color scale for III and IV is reduced to enable clearer comparison.

which highlights the temperature distribution on the gate metal. Figures 5b(I)–(II) compare the thick-channel devices on sapphire and AlN substrates, where the sapphire device shows a noticeably higher peak temperature. For the thin-channel devices (Figure 5b(III)–(IV)), the temperature contour scale is capped at 60°C to enable a more consistent comparison. Both the GRT measurement and the transient study indicate that the thermal challenges associated with using AlGaIn as a next-generation RF device material can be mitigated through substrate and channel engineering. In addition, further improvements in interfacial engineering and top-side cooling, such as integrating high- k materials, can provide additional thermal benefits. Although the thin-channel devices exhibited some degradation in electrical performance, they can be further optimized to achieve a balance between thermal management and electrical performance, ensuring overall device optimization [19].

3 Conclusion

This work examines how substrate and channel engineering can address the thermal challenges limiting the adoption of AlGaIn-based RF devices. Integrating a high- k material such as AlN as the substrate, together with a thin 5-nm AlGaIn channel, reduces the overall device thermal resistance by more than 88.7% compared to a 500-nm-thick AlGaIn channel on sapphire. The record-low thermal resistance achieved in AlGaIn devices is also comparable to that of GaN devices grown on SiC substrates. These findings demonstrate that through optimized substrate, interfacial, and channel engineering, AlGaIn RF devices can be designed to deliver improved thermal performance suitable for high-power and high-frequency operation.

4 Acknowledgments

This work was funded by ARO DEVCOM under the Grant No. W911NF2220163 (UWBG RF Center, program manager Dr. Tom Oder).

Conflict of Interest

The authors declare no conflict of interest.

References

- [1] Brianna Klein, Andrew Allerman, Andrew Armstrong, Mary Rosprim, Colin Tyznik, Yinxuan Zhu, Chandan Joishi, Chris Chae, and Siddharth Rajan. Al-rich algan transistors with regrown p-algan gate layers and ohmic contacts. *Advanced Materials Interfaces*, 12(2):2301080, 2025.
- [2] Albert G. Baca, Brianna A. Klein, Joel R. Wendt, Stefan M. Lepkowski, Christopher D. Nordquist, Andrew M. Armstrong, Andrew A. Allerman, Erica A. Douglas, and Robert J. Kaplar. RF Performance of Al_{0.85}Ga_{0.15}N/Al_{0.70}Ga_{0.30}N High Electron Mobility Transistors With 80-nm Gates. *IEEE Electron Device Letters*, 40(1):17–20, January 2019.
- [3] Seunghoon Shin, Hridibrata Pal, Jon Pratt, John Niroula, Yinxuan Zhu, Chandan Joishi, Brianna A. Klein, Andrew Armstrong, Andrew A. Allerman, Tomás Palacios, and Siddharth Rajan. High Breakdown Electric Field (> 5 MV/cm) in UWBG AlGa_N Transistors, April 2025. arXiv:2504.12685 [cond-mat].
- [4] Yinxuan Zhu, Andrew A. Allerman, Chandan Joishi, Jonathan Pratt, Agnes Maneesha Dominic Merwin Xavier, Gabriel Calderon Ortiz, Brianna A. Klein, Andrew Armstrong, Jinwoo Hwang, and Siddharth Rajan. Heterostructure and interfacial engineering for low-resistance contacts to ultra-wide bandgap AlGa_N. *Applied Physics Letters*, 126(6):062107, February 2025.
- [5] Albert G. Baca, Andrew M. Armstrong, Brianna A. Klein, Andrew A. Allerman, Erica A. Douglas, and Robert J. Kaplar. Al-rich AlGa_N based transistors. *Journal of Vacuum Science & Technology A*, 38(2):020803, January 2020.
- [6] Sukwon Choi, Samuel Graham, Srabanti Chowdhury, Eric R. Heller, Marko J. Tadjer, Gilberto Moreno, and Sreekanth Narumanchi. A perspective on the electro-thermal co-design of ultra-wide bandgap lateral devices. *Applied Physics Letters*, 119(17):170501, October 2021.
- [7] Bikramjit Chatterjee, Daniel Shoemaker, Hiu-Yung Wong, and Sukwon Choi. Algan/gan hemt device physics and electrothermal modeling. In *Thermal Management of Gallium Nitride Electronics*, pages 103–163. Elsevier, 2022.
- [8] Seokjun Kim, Eungkyun Kim, Husam Walwil, Daniel C. Shoemaker, Jimmy Encomendero, Matthew T. DeJarld, Maher B. Tahhan, Eduardo M. Chumbes, Jeffrey R. Laroche, Debdeep Jena, Huili G. Xing, and Sukwon Choi. Thermal Characterization and Design of AlN/GaN/AlN HEMTs on Foreign Substrates. *IEEE Electron Device Letters*, 46(5):817–820, May 2025.
- [9] Henry T. Aller, Thomas W. Pfeifer, Alexander Chaney, Kent Averett, Thaddeus Asel, Zachary Engel, Asif Khan, Patrick Hopkins, Alan Doolittle, Shin Mou, and Samuel Graham. The impact of device architecture on the thermal response of AlN/AlGa_N digital alloy field-effect transistors. *Applied Thermal Engineering*, 276:126677, October 2025.
- [10] Horacio C. Nohetto, Nicholas R. Jankowski, and Avram Bar-Cohen. The Impact of GaN/Substrate Thermal Boundary Resistance on a HEMT Device. In *Volume 10: Heat and Mass Transport Processes, Parts A and B*, pages 241–249, Denver, Colorado, USA, January 2011. ASME.
- [11] Bryan K. Schwitter, Anthony E. Parker, Simon J. Mahon, Anthony P. Fattorini, and Michael C. Heimlich. Impact of Bias and Device Structure on Gate Junction Temperature in AlGa_N/Ga_N-on-Si HEMTs. *IEEE Transactions on Electron Devices*, 61(5):1327–1334, May 2014.
- [12] Henry T. Aller, Thomas W. Pfeifer, Abdullah Mamun, Kenny Huynh, Marko Tadjer, Tatyana Feygelson, Karl Hobart, Travis Anderson, Bradford Pate, Alan Jacobs, James Spencer Lundh, Mark Goorsky, Asif Khan, Patrick Hopkins, and Samuel Graham. Low Thermal Resistance of Diamond-AlGa_N Interfaces Achieved Using Carbide Interlayers. *Advanced Materials Interfaces*, n/a(n/a):2400575. _eprint: <https://onlinelibrary.wiley.com/doi/pdf/10.1002/admi.202400575>.
- [13] Naohiro Tsurumi, Hiroaki Ueno, Tomohiro Murata, Hidetoshi Ishida, Yasuhiro Uemoto, Tetsuzo Ueda, Kaoru Inoue, and Tsuyoshi Tanaka. AlN Passivation Over AlGa_N/Ga_N HFETs for Surface Heat Spreading. *IEEE Transactions on Electron Devices*, 57(5):980–985, May 2010.
- [14] Kazuyuki Hirama, Yoshitaka Taniyasu, and Makoto Kasu. AlGa_N/Ga_N high-electron mobility transistors with low thermal resistance grown on single-crystal diamond (111) substrates by metalorganic vapor-phase epitaxy. *Applied Physics Letters*, 98(16):162112, April 2011.

- [15] Md Didarul Alam, Mikhail Gaevski, Mohi Uddin Jewel, Shahab Mollah, Abdullah Mamun, Kamal Hussain, Richard Floyd, Grigory Simin, MVS Chandrashekhar, and Asif Khan. Excimer laser liftoff of AlGa_N/Ga_N HEMTs on thick AlN heat spreaders. *Applied Physics Letters*, 119(13):132106, September 2021.
- [16] Samuel H. Kim, Daniel Shoemaker, Andrew J. Green, Kelson D. Chabak, Kyle J. Liddy, Samuel Graham, and Sukwon Choi. Transient Thermal Management of a β -Ga₂O₃ MOSFET Using a Double-Side Diamond Cooling Approach. *IEEE Transactions on Electron Devices*, 70(4):1628–1635, April 2023. Conference Name: IEEE Transactions on Electron Devices.
- [17] Abdullah Mamun, Kamal Hussain, Richard Floyd, MD Didarul Alam, MVS Chandrashekhar, Grigory Simin, and Asif Khan. Al_{0.64}Ga_{0.36}N channel MOSHFET on single crystal bulk AlN substrate. *Applied Physics Express*, 16(6):061001, June 2023. Publisher: IOP Publishing.
- [18] Seunghoon Shin, Can Cao, Jon Pratt, Yinxuan Zhu, Brianna A. Klein, Andrew Armstrong, Andrew A. Allerman, and Siddharth Rajan. Barrier electrostatics and contact engineering for ultra-wide bandgap algan hfets. *APL Electronic Devices*, 1(4), December 2025.
- [19] Yinxuan Zhu, Andrew A. Allerman, Ashley Wissel-Garcia, Seunghoon Shin, Jon Pratt, Can Cao, Kyle J. Liddy, James S. Speck, Brianna A. Klein, Andrew Armstrong, and Siddharth Rajan. Ultra-wide bandgap algan heterostructure field effect transistors with current gain cutoff frequency above 85 ghz. 2025.
- [20] Georges Pavlidis, Brian Foley, and Samuel Graham. Gate resistance thermometry: An electrical thermal characterization technique. In *Thermal Management of Gallium Nitride Electronics*, pages 201–221. Elsevier, 2022.
- [21] Kazuyuki Hirama, Makoto Kasu, and Yoshitaka Taniyasu. RF High-Power Operation of AlGa_N/Ga_N HEMTs Epitaxially Grown on Diamond. *IEEE Electron Device Letters*, 33(4):513–515, April 2012.
- [22] Marko J. Tadjer, Travis J. Anderson, Mario G. Ancona, Peter E. Raad, Pavel Komarov, Tingyu Bai, James C. Gallagher, Andrew D. Koehler, Mark S. Goorsky, Daniel A. Francis, Karl D. Hobart, and Fritz J. Kub. Ga_N-On-Diamond HEMT Technology With TAVG = 176°C at PDC,max = 56 W/mm Measured by Transient Thermoreflectance Imaging. *IEEE Electron Device Letters*, 40(6):881–884, June 2019.
- [23] G. Pavlidis, M. S. Jamil, D. Myren, S. Keebaugh, J. Chang, M. Doerflein, S. Afroz, R. S. Howell, and A. Centrone. Thermal engineering increases current density in AlGa_N/Ga_N superlattice devices. *Applied Physics Letters*, 125(1):012103, July 2024.
- [24] Ryo Kagawa, Zhe Cheng, Keisuke Kawamura, Yutaka Ohno, Chiharu Moriyama, Yoshiki Sakaida, Sumito Ouchi, Hiroki Uratani, Koji Inoue, Yasuyoshi Nagai, Naoteru Shigekawa, and Jianbo Liang. High Thermal Stability and Low Thermal Resistance of Large Area Ga_N/3C-SiC/Diamond Junctions for Practical Device Processes. *Small*, 20(13):2305574, 2024. _eprint: <https://onlinelibrary.wiley.com/doi/pdf/10.1002/sml.202305574>.
- [25] Bikramjit Chatterjee, James Spencer Lundh, Yiwen Song, Daniel Shoemaker, Albert G. Baca, Robert J. Kaplar, Thomas E. Beechem, Christopher Saltonstall, Andrew A. Allerman, Andrew M. Armstrong, Brianna A. Klein, Anushka Bansal, Hamid R. Seyf, Disha Talreja, Alexej Pogrebnyakov, Eric Heller, Venkatraman Gopalan, Asegun S. Henry, Joan M. Redwing, Brian Foley, and Sukwon Choi. Interdependence of Electronic and Thermal Transport in Al_xGa_{1-x}N Channel HEMTs. *IEEE Electron Device Letters*, 41(3):461–464, March 2020. Conference Name: IEEE Electron Device Letters.
- [26] Zhenyu Qu, Yinfei Xie, Tiancheng Zhao, Wenhui Xu, Yang He, Yongze Xu, Huarui Sun, Tianguai You, Genquan Han, Yue Hao, and Xin Ou. Extremely Low Thermal Resistance of β -Ga₂O₃ MOSFETs by Co-integrated Design of Substrate Engineering and Device Packaging. *ACS Applied Materials & Interfaces*, 16(42):57816–57823, October 2024. Publisher: American Chemical Society.
- [27] James Spencer Lundh, Cory Cress, Alan G. Jacobs, Zhe Cheng, Hannah N. Masten, Joseph A. Spencer, Kohei Sasaki, James Gallagher, Andrew D. Koehler, Keita Konishi, Samuel Graham, Akito Kuramata, Travis J. Anderson, Marko J. Tadjer, Karl D. Hobart, and Michael A. Mastro. Electrothermal enhancement of β -(Al_xGa_{1-x})₂O₃/Ga₂O₃ heterostructure field-effect transistors via back-end-of-line sputter-deposited AlN layer. *Journal of Applied Physics*, 136(22):224502, December 2024.
- [28] Georges Pavlidis, Dustin Kendig, Eric R. Heller, and Samuel Graham. Transient Thermal Characterization of AlGa_N/Ga_N HEMTs Under Pulsed Biasing. *IEEE Transactions on Electron Devices*, 65(5):1753–1758, May 2018. Conference Name: IEEE Transactions on Electron Devices.